Article

Cancer Cell

Neutrophils Oppose Uterine Epithelial Carcinogenesis via Debridement of Hypoxic Tumor Cells

Graphical Abstract

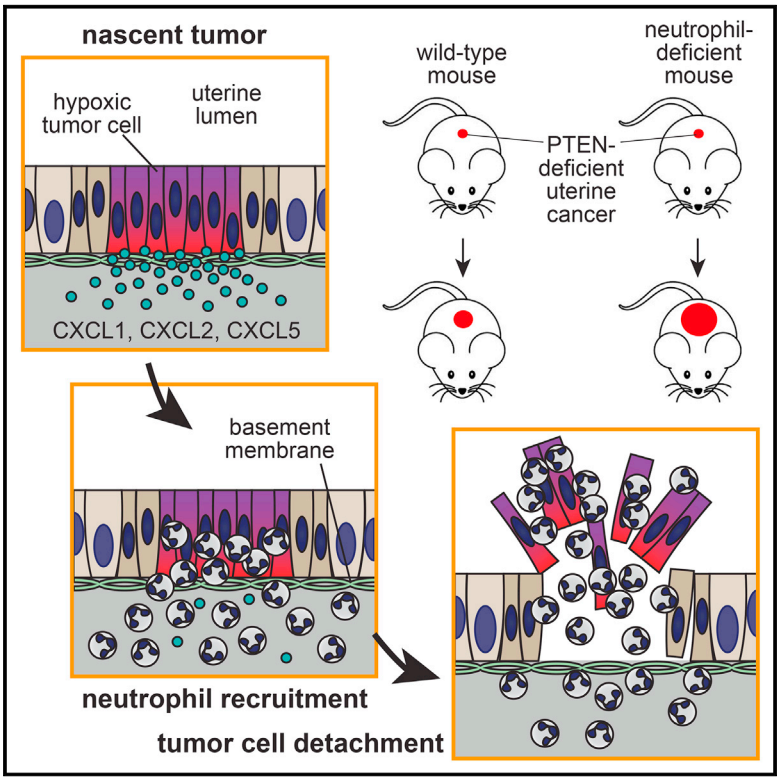

Authors

Adam Blaisdell, Amandine Crequer, Devin Columbus, Takiko Daikoku, Khush Mittal, Sudhansu K. Dey, Adrian Erlebacher

Correspondence

adrian.erlebacher@nyumc.org

In Brief

Blaisdell et al. show in a mouse model of uterine cancer that polymorphonuclear neutrophil (PMN) recruitment resulting from tumor hypoxia impedes early tumor growth and malignant progression. A PMN gene signature correlates with improved survival in multiple human cancer types.

Highlights

- PMNs slow tumor growth and malignant progression in PTEN-deficient uterine tumors
- PMNs reduce tumor burden by promoting tumor cell basement membrane detachment
- Anti-tumor PMN activity does not require other leukocytes or tumor cell senescence
- PMN recruitment to early-stage tumors is linked to hypoxia-induced inflammation

Accession Numbers

GSE73541

Blaisdell et al., 2015, Cancer Cell *28*, 785–799
December 14, 2015
http://dx.doi.org/10.1016/j.ccell.2015.11.005

Cancer Cell
Article

Neutrophils Oppose Uterine Epithelial Carcinogenesis via Debridement of Hypoxic Tumor Cells

Adam Blaisdell,[1] Amandine Crequer,[1] Devin Columbus,[1] Takiko Daikoku,[2,4] Khush Mittal,[1] Sudhansu K. Dey,[2] and Adrian Erlebacher[1,3,*]
[1]Department of Pathology, NYU School of Medicine, New York, NY 10016, USA
[2]Division of Reproductive Sciences, Cincinnati Children's Hospital Medical Center, Cincinnati, OH 45229, USA
[3]NYU Cancer Institute, NYU Langone Medical Center, New York, NY 10016, USA
[4]Present address: Division of Transgenic Animal Science, Advanced Science Research Center, Kanazawa University, Kanazawa 920-1192, Japan
*Correspondence: adrian.erlebacher@nyumc.org
http://dx.doi.org/10.1016/j.ccell.2015.11.005

SUMMARY

Polymorphonuclear neutrophils (PMNs) are largely considered to foster cancer development despite wielding an arsenal of cytotoxic agents. Using a mouse model of PTEN-deficient uterine cancer, we describe a surprising inhibitory role for PMNs in epithelial carcinogenesis. By inducing tumor cell detachment from the basement membrane, PMNs impeded early-stage tumor growth and retarded malignant progression. Unexpectedly, PMN recruitment and tumor growth control occurred independently of lymphocytes and cellular senescence and instead ensued as part of the tumor's intrinsic inflammatory response to hypoxia. In humans, a PMN gene signature correlated with improved survival in several cancer subtypes, including PTEN-deficient uterine cancer. These findings provide insight into tumor-associated PMNs and reveal a context-specific capacity for PMNs to directly combat tumorigenesis.

INTRODUCTION

Inflammation pervades virtually all forms of cancer even from the earliest stages of tumor development. Danger signals emanating from the tumor elicit local production of inflammatory cytokines and chemokines that subsequently draw inflammatory leukocytes into the neoplastic tissue. In general, inflammation is thought to nourish tumor growth and accelerate malignant progression (Trinchieri, 2012). However, certain inflammatory effectors within the tumor microenvironment remain functionally anti-tumor, particularly those that either block tumor cell proliferation or induce tumor cell death. Harnessing the power of these effectors represents a significant therapeutic challenge and requires a better understanding of the pathways that govern tumor-associated inflammation.

Polymorphonuclear neutrophils (PMNs) rapidly and ubiquitously infiltrate inflamed tissue and thus likely dominate even the earliest interactions of the host immune system with a nascent tumor. In line with the literature on tumor-associated inflammation, the vast majority of recent work on PMNs in cancer has ascribed to them pro-tumorigenic properties (Brandau et al., 2013). Tumor-associated PMNs have variously been shown to stimulate tumor cell proliferation, block cellular senescence, promote angiogenesis, and inhibit the tumor-associated adaptive immune response. On the other hand, activated PMNs robustly produce a variety of toxic compounds and can induce tumor cell cytolysis or cytostasis in vitro, which suggests that in certain circumstances they might oppose tumorigenesis (reviewed in Souto et al., 2011). Indeed, PMNs can inhibit growth of tumors engineered to recruit them in high numbers and have long been thought to be critical in vivo effectors of antibody-mediated tumor cell lysis (Albanesi et al., 2013; Souto et al., 2011). More recently, PMNs have been suggested to unleash the anti-tumor potential of cytotoxic T cells (Fridlender et al., 2009; Kousis et al., 2007) and to oppose seeding of metastatic tumor cells at distal tissue sites (Granot et al., 2011). Critically, all of this work employed transplantable tumor models, which thus leaves unaddressed the capacity of PMNs to combat primary, autochthonous tumorigenesis. Additionally, whether PMNs can resist cancer development independently of other immune cells or therapeutic manipulation remains unknown. These questions are particularly relevant to the early stages of tumorigenesis,

Significance

We present evidence in mice and humans that PMNs provide an endogenous defense mechanism against cancer of the uterus. Our work also unexpectedly suggests that PMNs are recruited to the tumor-bearing mouse uterus as a result of tumor hypoxia rather than anti-tumor adaptive immunity or tumor cell senescence. These results reveal an innate immune cell-mediated pathway of cancer resistance and support efforts to harness PMNs therapeutically to combat cancer.

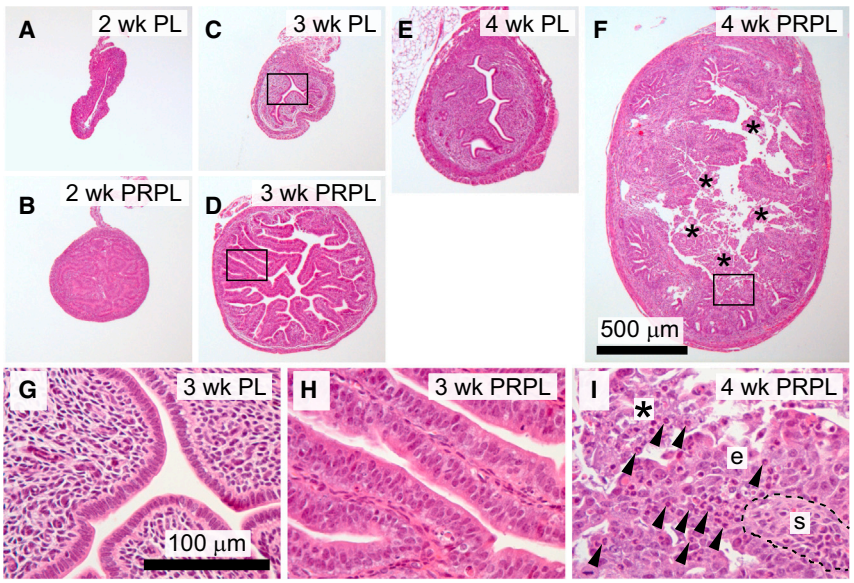

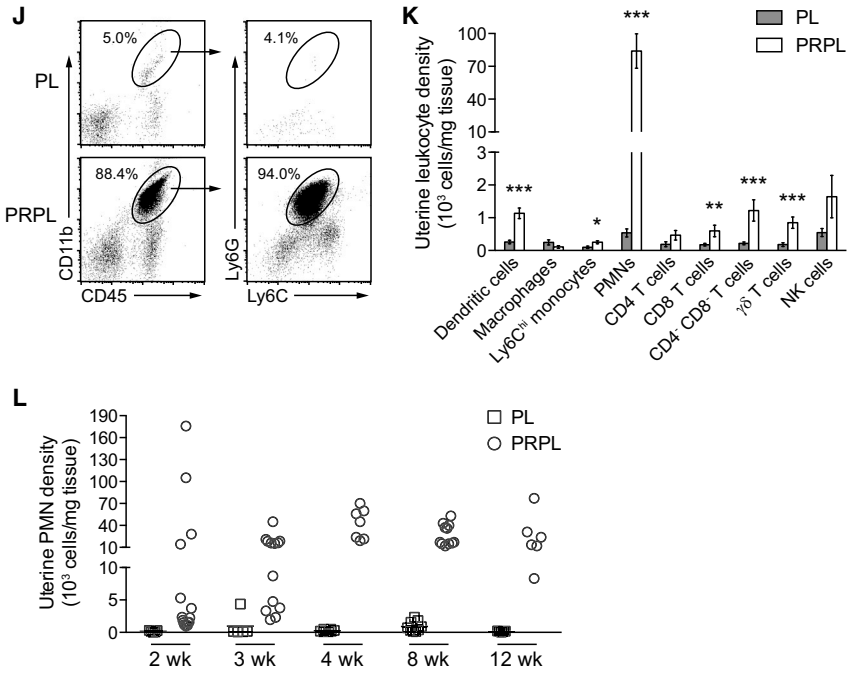

Figure 1. Appearance and Leukocytic Composition of Early-Stage PRPL Lesions

(A–I) Hematoxylin and eosin- (H&E) stained uterine cross sections from 2-, 3-, and 4-week-old (wk) PL and PRPL mice.

(G–I) Close-ups of boxed areas in (C), (D), and (F) (asterisk, intraluminal debris; arrowheads, inflammatory cells with multilobular nuclei; e, intact tumor epithelium; s, stroma). The images in (A)–(F) and (G)–(I) were taken at the same respective magnifications.

(J) Representative flow cytometric analyses of 4-week uteri. The plots on the left were gated on viable cells and display equal numbers of non-leukocytes ($CD45^-$).

(K) Leukocyte subset densities in 4-week uteri, as determined by flow cytometry (mean ± SEM of $n \geq 5$ mice per group) (*$p < 0.05$; **$p < 0.01$; and ***$p < 0.005$).

(L) Uterine PMN tissue densities through the course of PRPL tumor development, as determined by flow cytometry.

See also Figure S1.

when PMNs might be uniquely positioned to influence tumor outcome.

Here, we investigated the role of PMNs during development of the endometrioid subtype of endometrial adenocarcinoma (EC), the most common form of uterine cancer and the most prevalent gynecological malignancy in American women (Di Cristofano and Ellenson, 2007). This cancer is frequently (>50% of cases) associated with functional loss of the tumor suppressor PTEN. Our studies primarily relied upon a genetic model of this cancer in which cre recombinase expression under control of the progesterone receptor (PR) promoter drives conditional *Pten* deletion within the uterus (Daikoku et al., 2008). These PR-cre ($Pgr^{cre/+}$) $Pten^{lox/lox}$ mice, referred to here as "PRPL" mice, develop fully penetrant endometrial cancer with characteristically rapid and synchronous progression throughout the entire uterus, thus providing a powerful model to study how PMNs respond to an epithelial cancer at its earliest stages of development.

RESULTS

PMN Recruitment into Early-Stage PRPL Tumors Correlates with Dramatic Changes in Tumor Morphology

The basic oncological features of PRPL mice have been described using mice on a mixed genetic background (Daikoku et al., 2008). To facilitate studying their immunological features, we generated PRPL mice on a C57BL/6 background. Littermate females lacking the cre recombinase ("PL" mice) served as non-tumor-bearing controls. As expected, the uteri of 2-week-old PRPL mice showed uniform uterine epithelial hyperplasia (Figures 1A and 1B) and accumulation of phosphorylated AKT (pAKT), an indicator of PTEN inactivation, within all epithelial cells (Figure S1A). At 3 weeks, nearly all PRPL uteri displayed an extension of the 2-week phenotype, with the hyperplastic epithelium forming papillary structures containing scant amounts of underlying stroma (Figures 1C, 1D, 1G, and 1H). In stark contrast, the uteri of all 4-week-old PRPL mice exhibited a highly disorganized endometrium characterized by irregular epithelial surfaces, a prominent stroma, and large amounts of intraluminal cellular debris (Figures 1F and 1I). Such debris was never observed in the uteri of 4-week-old PL mice (Figure 1E), consistent with their pre-pubertal age and the lack of endometrial shedding during the murine estrus cycle.

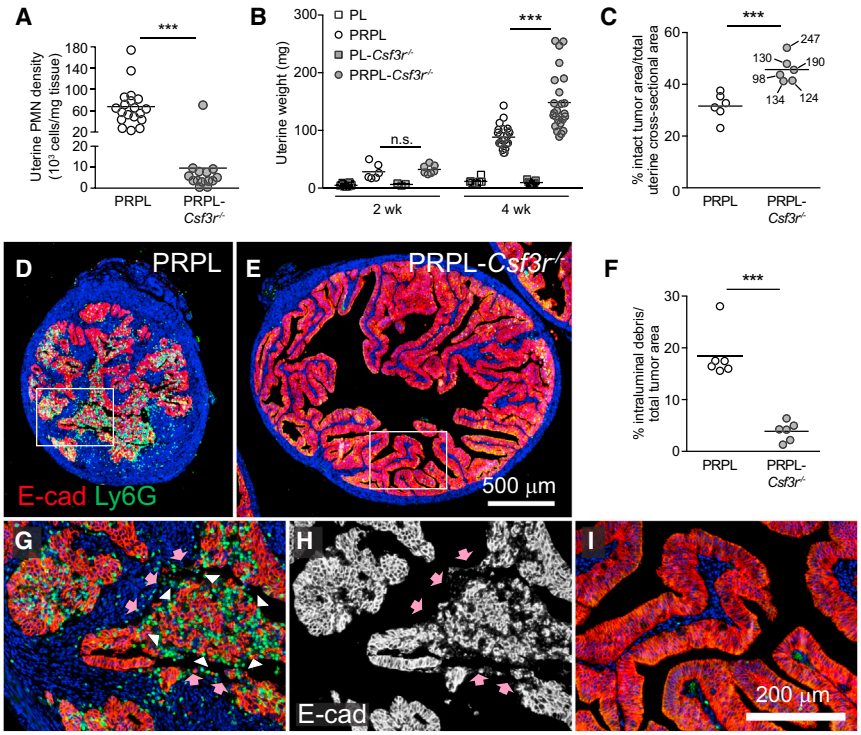

Figure 2. Effect of PMN Depletion on the Growth and Appearance of Early-Stage PRPL Tumors

(A) Uterine PMN densities in 4-week-old mice, as determined by flow cytometry.

(B) Uterine weights in 2- and 4-week-old mice.

(C) Percent cross-sectional area in 4-week uteri occupied by the intact E-cadherin (E-cad)$^+$ tumor epithelium, a measure of the proportion of the uterus occupied by living tumor. Each PRPL-*Csf3r*$^{-/-}$ data point is marked with corresponding uterine weight (mg), demonstrating the independence of these two parameters.

(D and E) Representative 4-week uterine tissue sections co-stained for E-cad to identify tumor cells and Ly6G to identify PMNs (n = 6 mice per group).

(F) Prevalence of intraluminal debris in 4-week tumors quantified as a percentage of total tumor area (intact epithelium + debris).

(G–I) Close-ups of the boxed areas in (D) and (E). (H) Shows E-cad staining alone to highlight the appearance of the intraluminal debris (white arrowheads in G) (pink arrows: surface of denuded stroma) (***$p < 0.005$ and not significant, n.s.).

See also Figure S2.

The rapid morphological change in 4-week PRPL uteri was accompanied by an influx of inflammatory leukocytes, many of which had the characteristic multilobular nuclei of mature PMNs and inhabited both the epithelium and intraluminal debris (Figure 1I). Indeed, examination of 4-week PRPL uteri by flow cytometry revealed substantial numbers of CD45$^+$ leukocytes expressing the myeloid lineage marker CD11b and high levels of Ly6G, a specific marker of PMNs in mice (Figures 1J and S1B). These cells moreover expressed intermediate levels of Ly6C (Figure 1J), but negligible levels of MHCII, CD11c, and F4/80 (Figure S1C), thus differentiating them from uterine Ly6C^{hi} monocytes, dendritic cells (DCs), and macrophages (Tagliani et al., 2011) and confirming their identity as PMNs. They furthermore produced reactive oxygen species (ROS) and IL-1β (Figures S1D–S1F), consistent with an activated state. Although 4-week PRPL uteri harbored increased tissue densities of other leukocyte subsets, PMNs were by far the dominant population, comprising ~90% of all uterine leukocytes (Figure 1K). The proportion of PRPL mice with substantially elevated uterine PMN numbers progressively increased from ~25% at 2 weeks to ~60% at 3 weeks to 100% at 4 weeks and older (Figure 1L). Together, these results indicated that PRPL tumors started to recruit PMNs when the mice were 2–3 weeks old, immediately prior to their striking shift in morphology.

PMN Depletion Enhances the Growth of Early-Stage PRPL Lesions

To determine whether PMNs affected PRPL tumorigenesis, we generated PRPL-*Csf3r*$^{-/-}$ mice deficient in the receptor for the PMN growth and survival factor G-CSF. *Csf3r*$^{-/-}$ mice have systemically low PMN numbers (Liu et al., 1996), and 4-week-old PRPL-*Csf3r*$^{-/-}$ mice accordingly exhibited a profound (>80%) reduction in uterine and blood PMNs (Figures 2A and S2A) when compared to PRPL mice. In contrast, the densities of other uterine leukocyte subsets in PRPL-*Csf3r*$^{-/-}$ tumors were not significantly reduced (Figure S2B). Remarkably, PRPL-*Csf3r*$^{-/-}$ uteri also demonstrated significantly increased (~2.6-fold) tumor burden, as evidenced by an increase in both uterine weight (Figure 2B) and the proportion of uterus occupied by intact tumor epithelium (Figure 2C; see also Figure 4E). In addition, 4-week PRPL-*Csf3r*$^{-/-}$ uteri displayed the organized papillary architecture distinctive of 3-week PRPL uteri (Figures 2E and 2I) rather than the disorganized epithelium characteristic of 4-week PRPL uteri (Figures 2D and 2G).

Importantly, 2- to 3-week-old PRPL and PRPL-*Csf3r*$^{-/-}$ mice had similar uterine weights and tumor appearance (Figures 2B and S2C), arguing against a tumor cell-intrinsic role for G-CSFR in PRPL lesion development and, instead, temporally correlating the divergence of PRPL and PRPL-*Csf3r*$^{-/-}$ tumor size and morphology with the influx of PMNs. Furthermore, antibody-mediated G-CSF neutralization in PRPL mice recapitulated the reduction in blood and uterine PMNs, tumor size increase, and morphological alterations observed in 4-week-old PRPL-*Csf3r*$^{-/-}$ mice (Figures S2D–S2G), indicating that the PRPL-*Csf3r*$^{-/-}$ phenotype was not due to a developmental defect in *Csf3r*$^{-/-}$ mice. Together, these results suggested that PMNs inhibited PRPL tumor growth during the early stages of progression and induced the transition in tumor morphology that occurred between 3 and 4 weeks of age.

PMNs Restrict PRPL Tumor Growth by Inducing Tumor Cell Detachment from the Basement Membrane

We next evaluated the mechanisms by which PMNs reduced early-stage PRPL tumor burden. Strikingly, the increased tumor

burden of 4-week PRPL-*Csf3r*$^{-/-}$ uteri correlated with a dramatic reduction in their content of intraluminal debris (Figure 2F). In 4-week PRPL uteri, this debris appeared disaggregated and, in addition to numerous Ly6G^{+} PMNs, contained E-cadherin^{+} tumor cells (Figures 2G and 2H) that frequently showed signs of early necrosis (Figure S3A). However, many of the intraluminal tumor cells were still viable, as revealed by examination of uterine lavages (Figure 3A), and many had even incorporated BrdU injected 2 hr prior to sacrifice (Figure 3B), indicating that they were recently in S phase and thus had recently detached from the endometrium. Indeed, the debris was frequently adjacent to areas of stroma that were denuded of an overlying epithelium (arrows in Figures 2G, 2H, 3B, and 3C), yet remained covered with the laminin γ1 subunit, a ubiquitous basement membrane component (Figure 3C). Together, these results suggested that PMNs reduced PRPL tumor burden by promoting the basement membrane detachment of viable tumor cells. We will refer to this process as ''tumor cell sloughing''.

To further characterize this process, we assessed the epithelial expression and subcellular localization of the integrin $\alpha6\beta4$. This integrin is critical for anchoring epithelia to basement membranes, as many studies have demonstrated that an inability to generate stable, $\alpha6\beta4$-containing adhesion complexes within the basement membrane zone (BMZ) predisposes live epithelial cells to detachment (reviewed in Zhang and Labouesse, 2010). Remarkably, 4-week PL and PRPL-*Csf3r*$^{-/-}$ uteri showed extensive $\alpha6$ staining in a largely continuous pattern throughout the epithelial BMZ, whereas the epithelial BMZ in PRPL uteri contained only rare and discontinuous stretches of concentrated $\alpha6$ (Figures 3D–3G). The $\beta4$ staining pattern in PRPL uteri was similarly altered (Figures S3B and S3C). PRPL and PRPL-*Csf3r*$^{-/-}$ tumor cells nevertheless expressed equivalent total surface levels of $\alpha6$ and $\beta4$—albeit both lower than observed in PL epithelial cells—as well as of $\beta1$ (a separate $\alpha6$ integrin binding partner; Figure 3H), indicating that the reduced epithelial BMZ staining of $\alpha6$ and $\beta4$ in PRPL uteri was due to impaired $\alpha6\beta4$ basolateral polarization rather than to diminished expression. These observations linked PMN infiltration and tumor cell sloughing to $\alpha6\beta4$ adhesion complex disassembly in the BMZ and thus to a reduction in cell adhesiveness to the basement membrane.

Importantly, PMNs are thought to induce epithelial cell detachment from basement membranes in models of autoimmunity, infection, and environmental tissue damage, and indeed produce ROS and a wide spectrum of proteases that can degrade BMZ components (Johnston et al., 2005; Liu et al., 2000; Molloy et al., 2013; Owen and Campbell, 1999; Riedle and Kerjaschki, 1997; Venaille et al., 1995). However, to our knowledge, PMN-induced epithelial detachment has not been reported in cancer. Instead, previous examples of PMN-opposed tumor growth have implicated CD8 T cells as the direct effectors of tumor cell death or have relied upon tumor cell targeting by B cell-generated antibodies (Fridlender et al., 2009; Kousis et al., 2007; Souto et al., 2011). We therefore assessed the potential roles of other leukocytes in PRPL tumorigenesis. Remarkably, PRPL mice genetically deficient in B and T cells (PRPL-*Rag2*$^{-/-}$) and mice additionally deficient in innate lymphocytes (PRPL-*Rag2*$^{-/-}$*Il2rg*$^{-/-}$) showed no significant changes in uterine PMN density, weight, tumor burden, or sloughing when compared to 4-week-old PRPL mice (Figures 3I–3L, S3D, and S3E). Similar results were obtained with PRPL mice deficient in DCs or monocytes and macrophages (see below). These results indicated that PMNs were the principal effector cells that opposed PRPL tumor growth and induced tumor cell sloughing.

We also assessed whether PMNs might additionally inhibit PRPL tumor growth by opposing tumor cell proliferation, a possibility raised by their known cytostatic properties in vitro (Souto et al., 2011). However, 4-week PRPL tumor cells paradoxically proliferated more rapidly than their PRPL-*Csf3r*$^{-/-}$ counterparts, as evidenced by a higher percentage of cells expressing the M phase marker phospho-histone H3 (pH3; Figures S3F and S3G). This finding was supported by analyses of tumor cell size, RNA-sequencing (seq) data from sorted tumor cells, and the expression pattern of the cell cycle inhibitor p27^{kip1} (Figures S3H–S3O). We also could not find evidence that PMNs induced tumor cell apoptosis within the intact tumor epithelium, as both ex vivo flow cytometric assays and in situ histological analysis revealed similar levels of tumor cells expressing the apoptotic indicator cleaved caspase-3 in PRPL and PRPL-*Csf3r*$^{-/-}$ uteri (Figures S3P and S3Q). These levels were nevertheless greatly elevated over those for PL uterine epithelial cells. Collectively, these results implied that the induction of tumor cell sloughing was the primary, if not exclusive, means by which PMNs reduced PRPL tumor burden.

Opposition to PRPL Tumor Growth Involves Myd88-Dependent PMN Activation

We also observed PMN-induced tumor cell sloughing in an alternate model of PTEN-deficient uterine cancer in which, contrary to the PRPL model, tumorigenesis is initiated focally in adult mice with fully developed immune systems (Beauparlant et al., 2004). In this model, hereafter referred to as ''PL-AdCre'', injection of cre-expressing adenoviral vectors into the uterine lumen of 6-week-old PL mice generated discrete pAKT^{+} papillary structures with the hyperplastic morphology of 3-week PRPL uteri (Figures 4A and S4A–S4C). At 10–14 days post-injection (dpi), many of these pAKT^{+} lesions, like their PRPL counterparts, became infiltrated with PMNs and sloughed into the uterine lumen, which in this model left behind stretches of normal pAKT^{-} epithelium (Figures 4A, arrowheads, and S4A–S4C).

Interestingly, some papillary lesions in 14 dpi PL-AdCre uteri showed no evidence of tumor cell sloughing despite PMN infiltration (Figure 4A, asterisk). This observation was reminiscent of the many 3-week PRPL uteri with both papillary morphology and PMN infiltration (Figures 1H and 1L; see also Figure 7B) and suggested that PMNs required a distinct intratumoral activation signal to induce tumor cell sloughing. Indeed, we also noticed that the uterine PMNs of 4-week-old PRPL mice deficient in the signaling adaptor MyD88 (PRPL-*Myd88*$^{-/-}$), a known regulator of PMN activation with multiple downstream effects (Prince et al., 2011), produced significantly lower levels of ROS and IL-1β compared to their PRPL counterparts (Figures 4B and 4C). Critically, PRPL-*Myd88*$^{-/-}$ uteri also showed decreased tumor cell sloughing accompanied by an ~2.4-fold increase in tumor burden (Figures 4E–4G, S4H, and S4I). These findings could not be easily ascribed to a change in uterine PMN tissue density (Figure 4D) nor to a PMN developmental defect, as

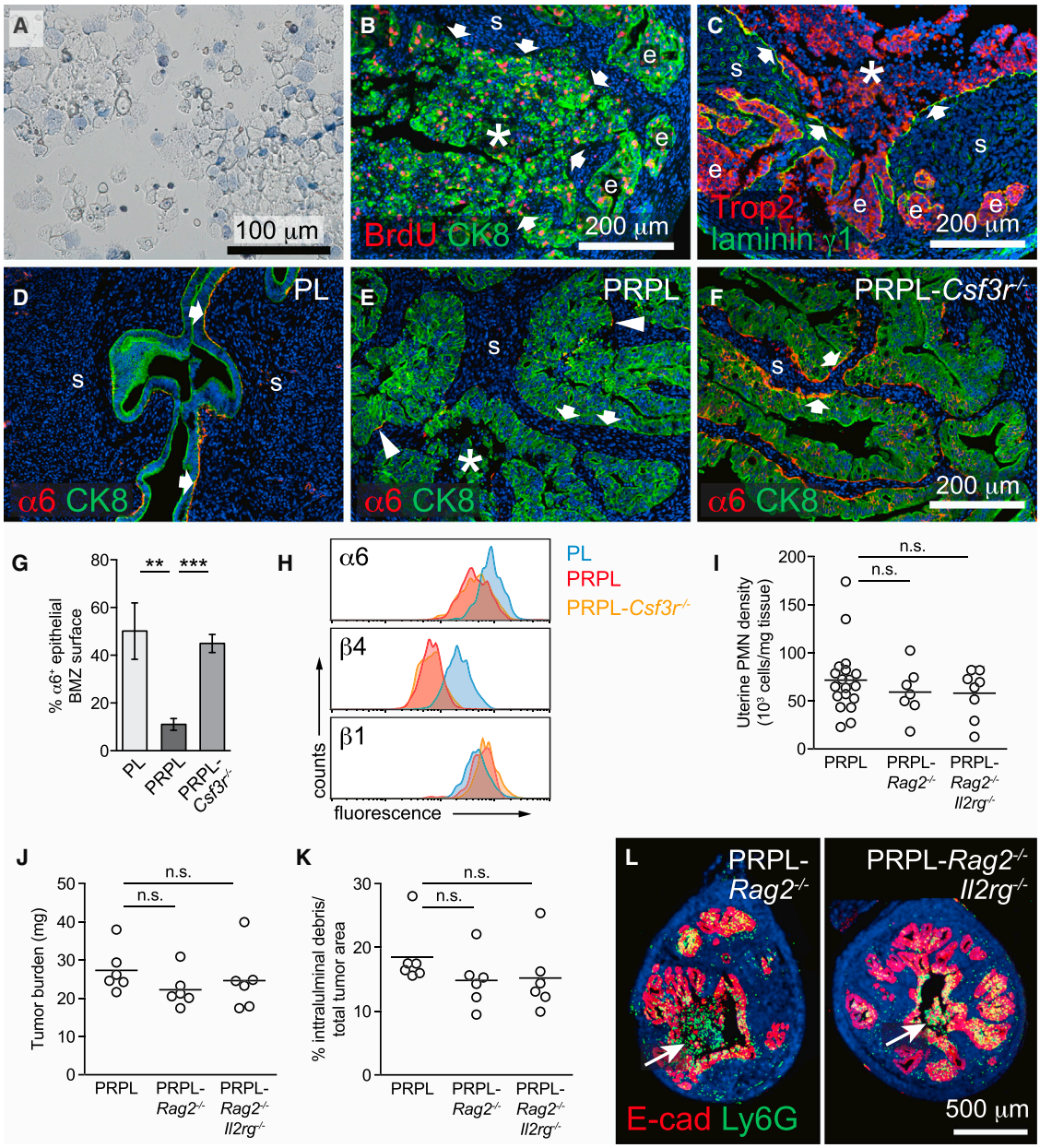

Figure 3. PMNs Directly Induce Basement Membrane Detachment of Viable Tumor Cells

(A) Representative cytospin preparation of the uterine lavage of a 4-week-old PRPL mouse stained with trypan blue to identify dead (blue) cells (n = 4). There was no material that could be flushed out of 4-week PL uteri.

(B) Representative section of a 4-week PRPL uterus stained for BrdU injected 2 hr prior to sacrifice and CK8 to identify epithelial cells (n = 6 mice). The arrows mark the periphery of a large area of intraluminal debris (asterisk). (e, intact tumor epithelium; s, stroma).

(C) Representative section of a 4-week PRPL uterus stained for the uterine epithelial marker Trop2 and laminin γ1 (n = 3 mice). The arrows indicate segments of the denuded stromal surface covered with laminin γ1.

(D–G) Representative 4-week uterine tissue sections co-stained for α6 and CK8 and quantified percentage of the epithelial BMZ positive for α6 staining (mean ± SEM of n = 6 mice per group). The arrows indicate the BMZ and the arrowheads indicate two small $\alpha6^{+}$ stretches.

(H) Flow cytometric analysis of integrin subunit expression on gated epithelial ($CD45^{-}EpCAM^{hi}$; see Figure S3M) cells (representative histograms of n = 4 mice per group).

(I–K) Uterine PMN densities, tumor burden (uterine weight X percent cross-sectional area comprised of intact tumor epithelium), and intraluminal debris prevalence in 4-week-old mice. The PRPL data are the same as in Figure 2.

(L) Representative E-cad/CK8 co-stained uterine tissue sections. The arrows indicate intraluminal debris.

See also Figure S3.

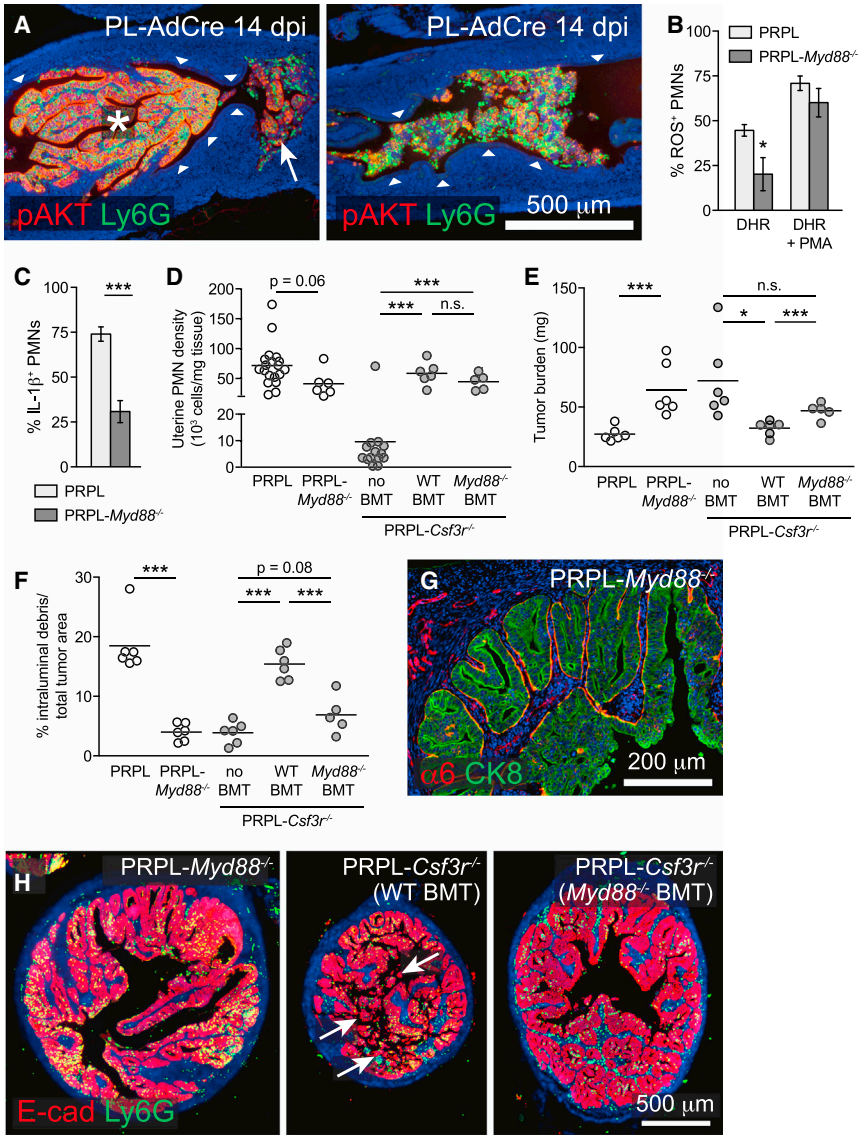

Figure 4. Tumor-Associated PMN Activation via a MyD88-Dependent Pathway

(A) Longitudinal sections from 14 dpi PL-AdCre uteri stained for Ly6G and pAKT to identify *Pten*-deleted epithelial cells. The white arrow shows the intraluminal debris comprised of tumor cells and PMNs. Intraluminal debris comprises the entirety of the tumor in the right image. The arrowheads show the normal pAKT$^-$ epithelium. The images are representative of n $\geq$ 5 mice per group.

(B and C) Uterine PMN production of ROS and IL-1β in 4-week-old PRPL and PRPL-*Myd88*$^{-/-}$ mice. The ROS production was assessed as in Figure S1D through the use of dihydrorhodamine (DHR); <1% of PMNs became fluorescent in the absence of this reagent.

(D–F) Uterine PMN densities, tumor burden, and intraluminal debris prevalence in 4-week-old PRPL, PRPL-*Myd88*$^{-/-}$, and PRPL-*Csf3r*$^{-/-}$ mice with or without the indicated BMT. The PRPL and PRPL-*Csf3r*$^{-/-}$ data are the same as in Figure 2.

(G) Representative α6/CK8 co-stained uterine tissue section from 4-week-old PRPL-*Myd88*$^{-/-}$ mice (n = 6).

(H) Representative E-cad/CK8 co-stained uterine tissue sections. The arrows indicate intraluminal debris. Of note, PRPL-*Csf3r*$^{-/-}$ (*Myd88*$^{-/-}$ BMT) uteri did not display pronounced papillary morphology.

See also Figure S4.

PRPL-*Myd88*$^{-/-}$ PMNs remained capable of producing ROS in response to PMA (Figure 4B) and expressed the developmental markers myeloperoxidase and MMP-9 (Figures S4D and S4E).

To more directly assess the role of MyD88-dependent PMN activation in PRPL tumorigenesis, we employed a bone marrow transfer (BMT) protocol to reconstitute the PMN compartment of PRPL-*Csf3r*$^{-/-}$ neonates with either wild-type (WT) or *Myd88*$^{-/-}$ cells. By 4 weeks of age, this protocol generated mice chimeric for multiple hematopoetic lineages (Figure S4F), but PMNs were singular in their greatly elevated uterine tissue density (Figures 4D and S4G). Importantly, PRPL-*Csf3r*$^{-/-}$ (WT BMT) uteri exhibited reduced tumor burden and enhanced tumor cell sloughing compared to PRPL-*Csf3r*$^{-/-}$ uteri, confirming the capacity of PMNs to oppose PRPL tumorigenesis (Figures 4E, 4F, and 4H). In contrast, PRPL-*Csf3r*$^{-/-}$ (*Myd88*$^{-/-}$ BMT) uteri maintained the high tumor burden seen in unmanipulated PRPL-*Csf3r*$^{-/-}$ uteri and showed low levels of tumor cell sloughing (Figures 4E, 4F, and 4H). These latter observations could not be attributed to MyD88 deficiency in other myeloid or lymphocyte subsets given the lack of impact of these other subsets on the PRPL phenotype, as discussed above. Together, these results suggested that efficient induction of tumor cell sloughing required Myd88-dependent PMN activation. Remarkably, PRPL-*Myd88*$^{-/-}$ uteri also exhibited the continuous BMZ staining pattern for the α6 integrin subunit seen in PRPL-*Csf3r*$^{-/-}$ uteri (Figure 4G; 45.0% ± 6.0% α6$^+$ epithelial BMZ surface), thus strengthening the link between α6β4 adhesion complex disassembly and tumor cell sloughing, while also indicating possible functions for the Myd88-dependent signal.

PMNs Inhibit the Malignant Progression of PRPL Tumors

We next addressed the role of PMNs in PRPL tumor progression. As shown in Figure 5A, the survival of PRPL-*Csf3r*$^{-/-}$ mice was reduced compared to PRPL mice. This effect could not be attributed to neutropenia per se since non-tumor-bearing PL and PL-*Csf3r*$^{-/-}$ mice demonstrated similar overall survival. Furthermore, an analysis of 12-week-old mice revealed that PRPL-*Csf3r*$^{-/-}$ tumors were significantly larger than PRPL tumors both in gross appearance (Figure 5B) and weight (Figure 5D), with an ~3.2-fold increase in total tumor burden (Figure 5E). Importantly, this increase was due not only to elevated tumor burden within the endometrium (Figure 5F), but also to substantial invasion of PRPL-*Csf3r*$^{-/-}$ tumors into the myometrium, an indicator of advancing tumor stage in human endometrial cancer

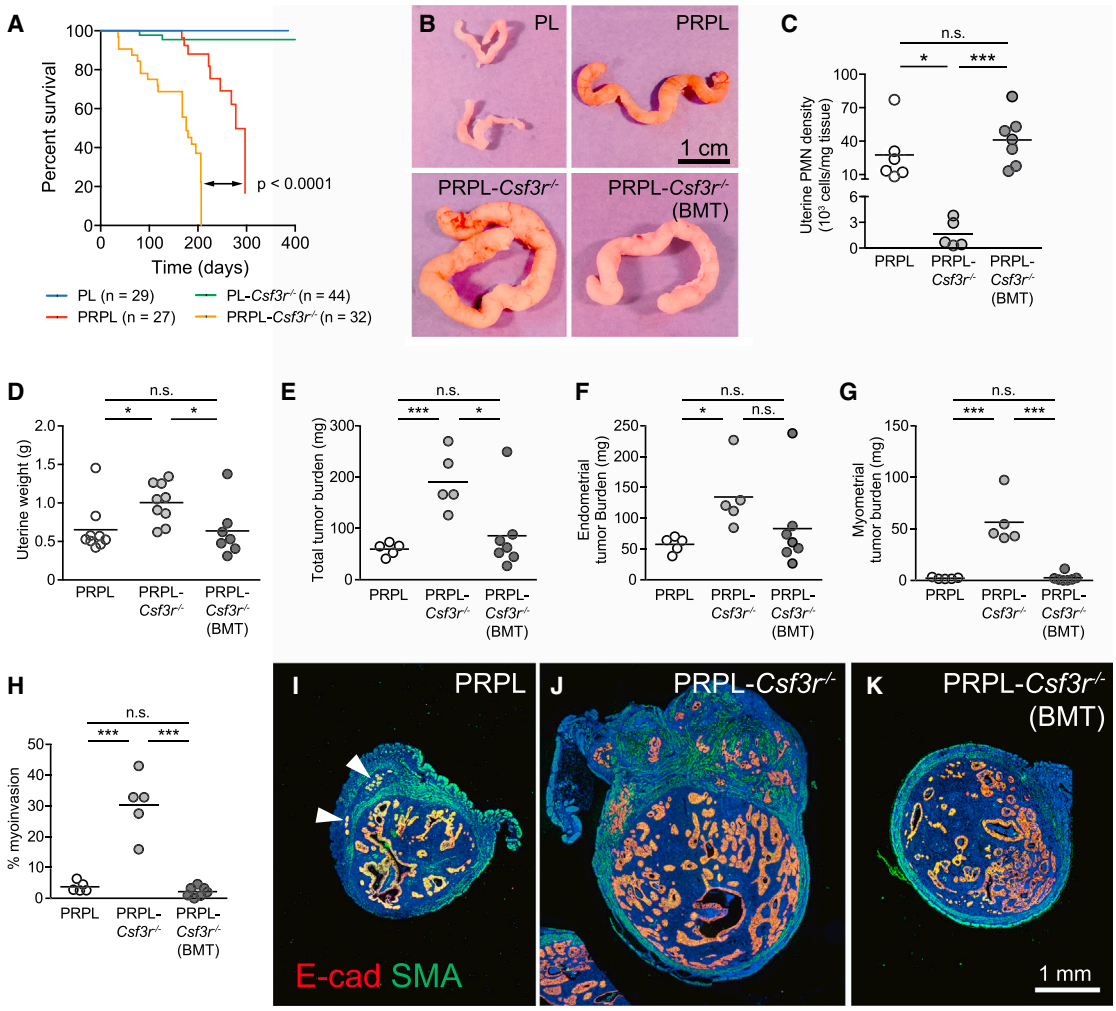

Figure 5. PMNs Retard Malignant Progression in PRPL Mice

(A) Survival curves.

(B–K) Analysis of 12-week uteri. (B) Representative gross appearance (n ≥ 5 mice per group); (C) PMN densities, as determined by flow cytometry; (D) weight; (E–G) tumor burden within (E) whole uteri, (F) endometrium alone, and (G) myometrium alone; (H) percent myoinvasion (% of cross-sectional tumor area within the myometrium); (I–K) representative cross sections co-stained for E-cad and smooth muscle actin (SMA) to identify myometrium (n ≥ 5 mice per group) (*p < 0.05; ***p < 0.005; arrowheads indicate myoinvasive foci).

See also Figure S5.

(Figures 5G–5J). Strikingly, use of neonatal BMT to reconstitute WT PMNs in PRPL-*Csf3r*$^{-/-}$ mice (Figures 5C, S5A, and S5B) nearly completely reverted this phenotype, with the resultant 12-week-old PRPL-*Csf3r*$^{-/-}$ (BMT) mice showing the same gross uterine appearance, weight, tumor burden, and percent myoinvasion as 12-week-old PRPL mice (Figures 5B and 5D–5K). These results demonstrated the powerful, long-term capacity of PMNs to restrain the growth and progression of PRPL tumors.

PMN Recruitment into PRPL Lesions Requires CXCR2 and Occurs Independently of Tissue-Resident Immune Cells, Commensal Microbes, and Tumor Cell Senescence

Given the pronounced and sustained influence of PMNs over PRPL tumorigenesis, we investigated the mechanisms governing PMN recruitment into PRPL tumors. Compared to age-matched PL controls, 4-week PRPL uteri demonstrated 50- to 900-fold elevations in mRNA expression of *Cxcl1*, *Cxcl2*, and *Cxcl5*—genes encoding the so-called "ELR-CXC" chemokines that specifically and potently attract PMNs via ligation of CXCR2—as well as other pro-inflammatory genes (*Il1a*, *Tnf*, *Il6*, *Ccl20*, and *Ptgs2*) and genes predominantly expressed by PMNs (*Il1b*, *Cxcr2, S100a8*, and *S100a9*) (Figure 6A). In contrast, 2-week PRPL uteri displayed <10-fold increased expression of these genes (Figure 6A). Remarkably, PRPL tumor cells themselves robustly expressed many of these genes—including *Cxcl1*, *Cxcl2*, and *Cxcl5*—at levels that rivaled those of housekeeping (*Actb* and *Gapdh*) and epithelium-specific genes (*Cdh1*, *Epcam*, and *Krt8*; Figure 6B). Immunostaining for CXCL5 confirmed its epithelium-specific expression in 4-week PRPL uteri (see Figures 7D, S7E, and S7H). Strikingly, PMN

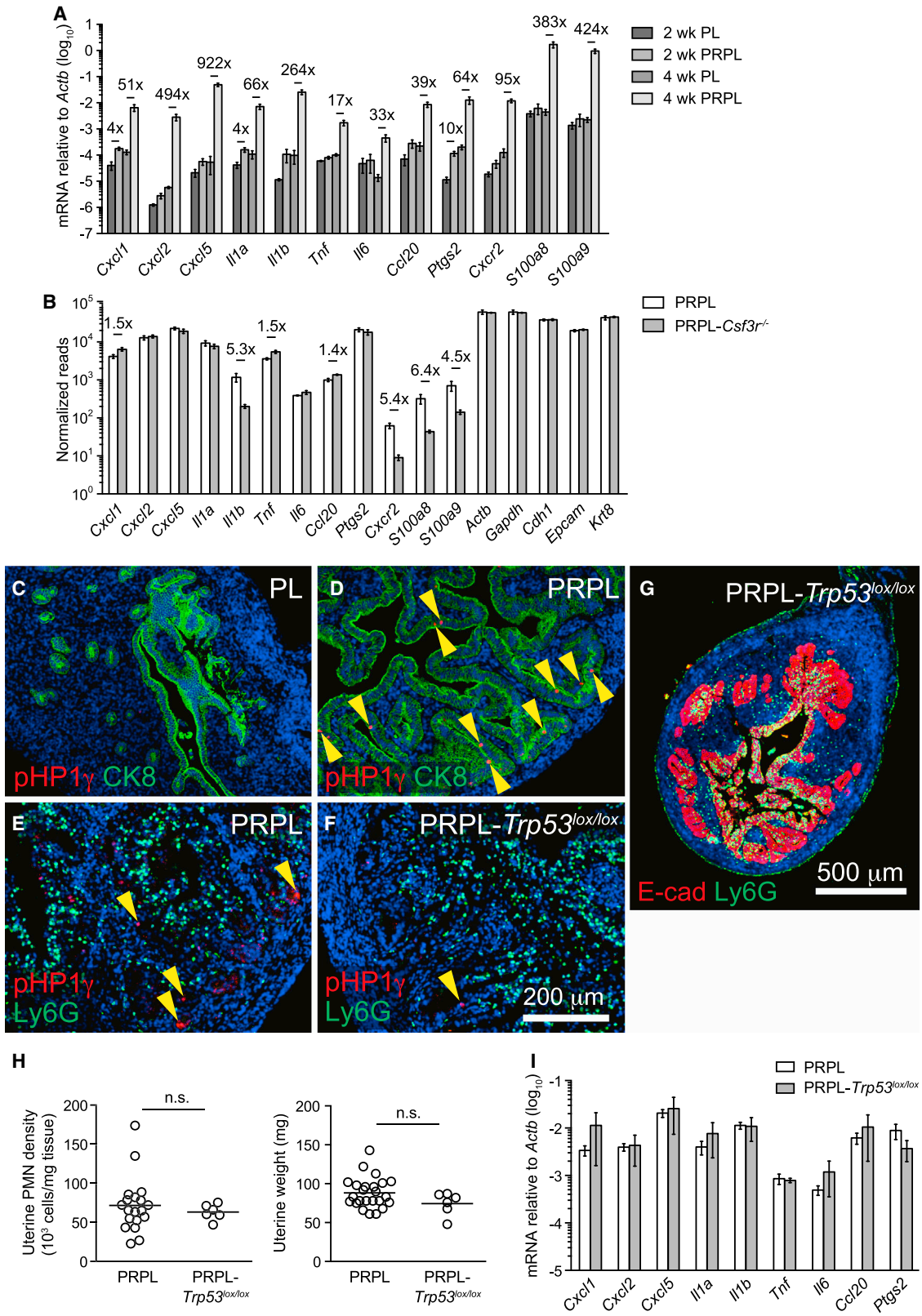

Figure 6. Inflammation and PMN Recruitment in PRPL Tumors Occurs Independently of Tumor Cell-Extrinsic Factors and Tumor Cell Senescence

(A) Quantitative (q)RT-PCR analysis of total uterine RNA from 2- and 4-week-old mice (mean ± SEM of n ≥ 4 mice per group). The genes with significant up-regulation ($p < 0.05$) are indicated by fold change.

(legend continued on next page)

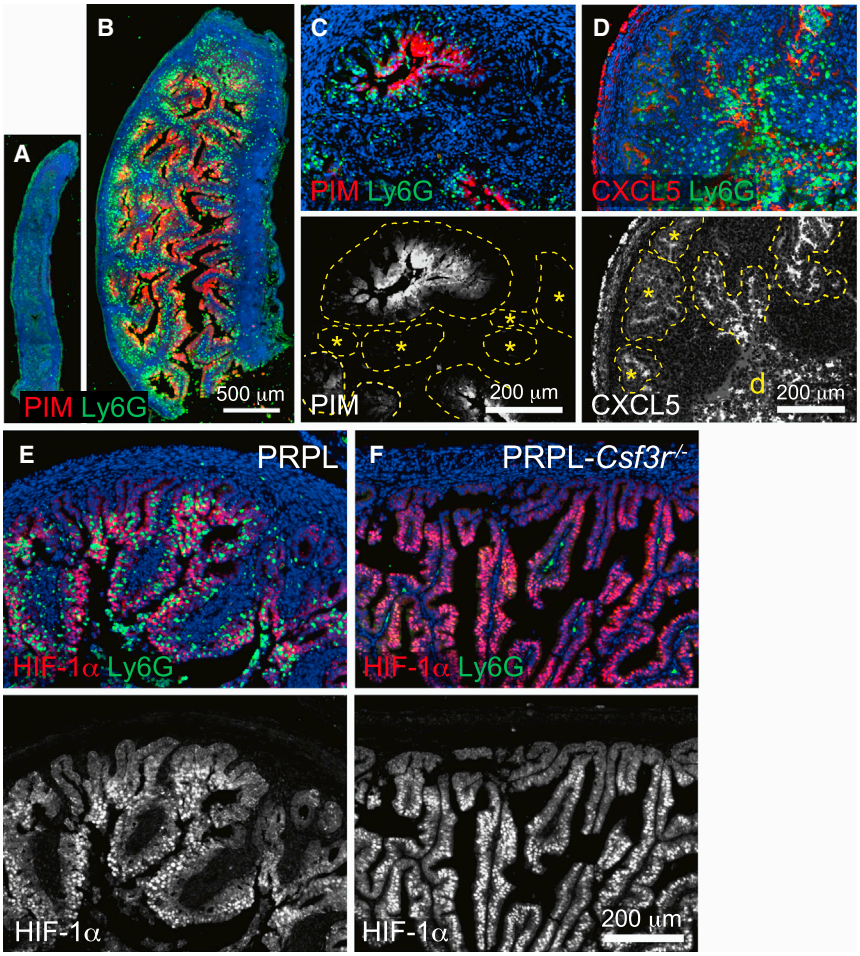

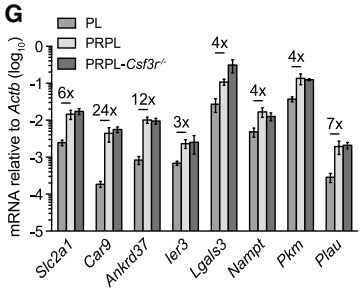

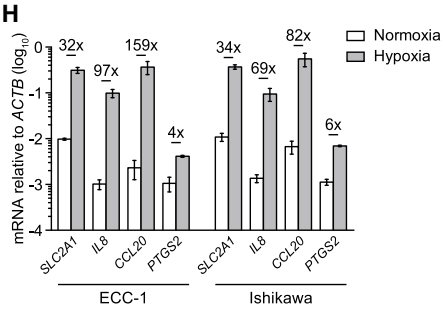

Figure 7. Inflammation and PMN Recruitment in PRPL Uteri Are Linked to Tumor Cell Hypoxia

(A and B) Representative longitudinal sections of 3-week uteri co-stained for PIM and Ly6G ($n \geq 3$ mice per group).

(C and D) Representative sections of 4-week PRPL uteri co-stained for Ly6G and either PIM (C) or CXCL5 (D) ($n = 3$ mice per group; d, intraluminal debris). The bottom images depict respective PIM or CXCL5 staining alone. The dashed lines outline the epithelium. The asterisks show epithelia largely devoid of PMNs and weakly positive for PIM and CXCL5.

(E and F) Representative 4-week sections co-stained for HIF-1α and Ly6G ($n = 3$ mice per group). Note the non-hypoxic (HIF-1α$^-$) epithelia at the periphery of both sections are also devoid of PMNs in the PRPL section. The bottom images depict HIF-1α staining alone to accentuate hypoxic versus non-hypoxic areas. The green cells within the stroma of (F) are autofluorescent RBCs.

(G) qRT-PCR analysis of hypoxia-induced genes in 4-week total uterine RNA (mean ± SEM of $n \geq 5$ mice per group). Fold changes that are significant ($p < 0.05$) are indicated.

(H) qRT-PCR analysis of hypoxia-induced and inflammatory gene expression by the ECC-1 and Ishikawa human EC cell lines cultured in normoxic (ambient O_2) or hypoxic (1% O_2) conditions. The representative data are from one of three independent experiments and the graphs show mean ± SEM of samples cultured in triplicate. Fold changes that are significant ($p < 0.05$) are indicated. See also Figure S7.

density and tumor cell sloughing were profoundly reduced in the uteri of 4-week-old PRPL mice deficient in CXCR2 (PRPL-*Cxcr2*$^{-/-}$), concomitant with increased uterine weight and tumor burden when compared to PRPL uteri (Figures S6A–S6F). Together, these results demonstrated the advent of a strong and generalized inflammatory stimulus between 2 weeks and 4 weeks in PRPL tumors that induced ELR-CXC chemokines critical for PMN recruitment.

As mentioned above, 4-week-old PRPL-*Rag2*$^{-/-}$ and completely alymphoid PRPL-*Rag2*$^{-/-}$*Il2rg*$^{-/-}$ mice showed no change in uterine tumor burden or PMN densities compared to PRPL mice (Figures 3I and 3J). Accordingly, their uterine inflammatory gene expression levels were also unchanged (Figure S6N). These data indicated that uterine-resident lymphocytes were dispensable for the tumor cell inflammatory response and PMN recruitment to the PRPL uterus. Similar results were obtained in PRPL mice deficient in DCs (PRPL-*Flt3l*$^{-/-}$) or macrophages and Ly6-C^{hi} monocytes (PRPL-αCSF-1R), as well as in PRPL mice given broad-spectrum antibiotics to deplete commensal microbes

(B) RNA-seq analysis from 4-week sorted tumor cells (mean ± SEM of n = 3–4 mice per group). The significant fold changes ($p < 0.05$) are indicated.

(C–F) Representative tissue sections from 2-week (C and D) or 4-week (E and F) uteri co-stained for pHP1γ and either CK8 (C and D) or Ly6G (E and F) ($n \geq 3$ mice per group). The yellow arrowheads show pHP1γ^{bright} senescent cells.

(G) Representative cross section of 4-week PRPL-*Trp53*$^{lox/lox}$ uterus co-stained for E-cad and Ly6G (n = 3 mice).

(H) Uterine PMN densities and weights of 4-week-old mice. The PRPL data are the same as in Figure 2.

(I) qRT-PCR analysis of 4-week total uterine RNA (mean ± SEM of n = 3–5 mice per group). There were no differences that were significant.

See also Figure S6.

(Figures S6F–S6O). Furthermore, despite their high level of IL-1β production, PMNs themselves were also dispensable for the tumor cell inflammatory response, as inflammatory gene expression in either whole uteri or sorted uterine epithelial cells from 4-week-old PRPL-*Csf3r*$^{-/-}$ mice was not decreased when compared to PRPL mice (Figures 6B and S6N). Notably, the ~5-fold elevation in *Il1b* expression within PRPL tumor cells could be attributed to a minor level of PMN contamination, consistent with the increased (4- to 6-fold), but low absolute expression of other PMN-specific genes (*Cxcr2*, *S100a8*, and *S100a9*) in these samples (Figure 6B).

Taken together, these results suggested that tumor cell-extrinsic factors did not drive the inflammatory response manifested by PRPL tumor cells. We therefore turned our attention to cellular senescence, a cell-intrinsic pathway activated in a p53-dependent manner following *Pten* loss in several cell types (including mouse epithelial cells; Chen et al., 2005; Daikoku et al., 2014) that can induce expression of many of the ELR-CXC and other inflammatory genes found to be upregulated in PRPL uteri (Coppé et al., 2010). Indeed, tumor cells expressing high levels of the senescence marker phospho-HP1γ (pHP1γ) were scattered throughout PRPL, but not PL uteri at 2 weeks of age (Figures 6C and 6D), suggesting that senescence occurred early in PRPL tumor development. However, the majority of 2-week PRPL uteri, such as the one shown in Figure 6D, lacked infiltrating PMNs (Figures 1L; see also S7A), demonstrating that senescence was not sufficient to induce uterine inflammation and PMN recruitment. Furthermore, the uteri of 4-week-old PRPL mice with conditional uterine deletion of p53 (PRPL-*Trp53*$^{lox/lox}$), while expectedly displaying a reduction in pHP1γ^{bright} tumor cells when compared to PRPL uteri (Figures 6E and 6F), showed no significant differences in uterine PMN density, weight, tumor morphology, or inflammatory gene expression (Figures 6G–6I). Thus, p53-dependent senescence was not required for early-stage inflammation or PMN recruitment.

Inflammation and PMN Recruitment Are Tightly Linked to Tissue Hypoxia in PRPL Tumors

In considering other tumor cell-intrinsic mechanisms for PMN recruitment, we were struck by the observation that both the PRPL and PL-AdCre models showed a significant delay between PTEN inactivation and PMN recruitment (Figures 1L, S4A, and S4B). Furthermore, PMNs within PL-AdCre uteri, which concurrently exhibited both large and small focal pAKT^{+} lesions at later time points, were restricted almost exclusively to the larger lesions (Figure S4A). These observations suggested that PMN recruitment was associated with increasing tumor size and thus possibly tumor hypoxia. Indeed, though hypoxia has not yet to our knowledge been described as a direct trigger of tumor-associated inflammation, inflammatory responses are common to many cell types under hypoxic conditions, including ELR-CXC chemokine production by non-transformed epithelial cells (Colgan et al., 1996; Eltzschig et al., 2014).

To explore this possibility, we first evaluated the spatial and temporal relationship in situ between PMN accumulation and pimonidazole adduct (PIM) formation, a direct biochemical indicator of severe hypoxia. At 2 weeks of age, both PL and PRPL uteri that lacked PMNs showed no obvious PIM^{+} staining (Figure S7A). In contrast, 3-week PRPL, but not PL uteri, exhibited broad PIM^{+} staining throughout the epithelium (Figures 7A and 7B) in association with the appearance of PMNs that, for the most part, had not yet infiltrated the epithelium. Moreover, hypoxic areas retaining a clear papillary morphology were generally PMN-free (Figure S7B). By 4 weeks of age, PRPL uteri had accumulated large numbers of intraepithelial PMNs that were co-localized with areas of intense PIM and CXCL5 staining (Figures 7C and 7D). Conversely, PIM^{-} and CXCL5^{-} epithelia were relatively devoid of PMNs (Figures 7C and 7D, asterisks, and S7C). PMN accumulation was also concentrated within segments of epithelium that showed nuclear accumulation of HIF-1α, a primary transcriptional mediator of the hypoxic response (Figure 7E). As expected, PL uterine epithelial cells lacked nuclear HIF-1α accumulation and stained negative for PIM and CXCL5 (Figures S7D–S7F). Together, these results indicated a tight association between uterine epithelial hypoxia, the uterine epithelial inflammatory response, and uterine PMN accumulation in PRPL tumors, with the onset of hypoxia appearing to slightly precede the infiltration of PMNs into the epithelium.

Importantly, PMN-deficient 4-week PRPL-*Csf3r*$^{-/-}$ uteri also featured large areas of nuclear HIF-1α accumulation within the epithelium (Figure 7F), as well as extensive epithelial segments that were PIM^{+} and CXCL5^{+} (Figures S7G and S7H). PRPL and PRPL-*Csf3r*$^{-/-}$ tumors also showed comparable transcriptional upregulation of hypoxia-induced genes evident both at the level of the whole tissue (Figure 7G) and in sorted tumor cells (Figure S7I). These results paralleled our data showing the independence of the tumor cell inflammatory response from PMN infiltration (Figure 6B) and together demonstrated that tumor hypoxia regulation did not require PMN infiltration. Indeed, hypoxic (1% O_2) exposure of two different human endometrial carcinoma (EC) cell lines with known PTEN deficiency (Weigelt et al., 2013) transcriptionally induced *IL8*—encoding the key human ELR-CXC chemokine IL-8—as well as other inflammatory genes (Figure 7H), thus demonstrating that hypoxia could induce an autonomous inflammatory response in transformed uterine epithelial cells.

A PMN Gene Signature Correlates with Improved Survival in Human Endometrioid EC and Other Cancer Subtypes

To extend our findings to human endometrioid EC and other human cancers, we took advantage of the paired clinical and RNA-seq data from The Cancer Genome Atlas (TCGA) to determine the extent to which tumor infiltration by PMNs influenced clinical outcome. Specifically, we examined correlations between patient survival and tumor expression of a gene signature (hereafter referred to as the "PMN signature") that reflected a tumor's propensity for PMN infiltration. The PMN signature was comprised of both PMN-specific genes (*CSF3R*, *CXCR2*, and *FCGR3B*) and genes encoding ELR-CXC chemokines. Compared to mice, humans express a larger array of ELR-CXC chemokines (*CXCL1*, *CXCL2*, *CXCL3*, *CXCL5*, *CXCL6*, *PPBP*, and *IL8*) that nevertheless remain functionally redundant for PMN recruitment. We therefore created an additional parameter— "SUM-6"—that represented the sum expression of these chemokines (excluding *PPBP* due its low overall expression and survival impact; Figure 8B) and thus the potential capacity of a tumor to recruit PMNs. Importantly, in endometrioid EC and

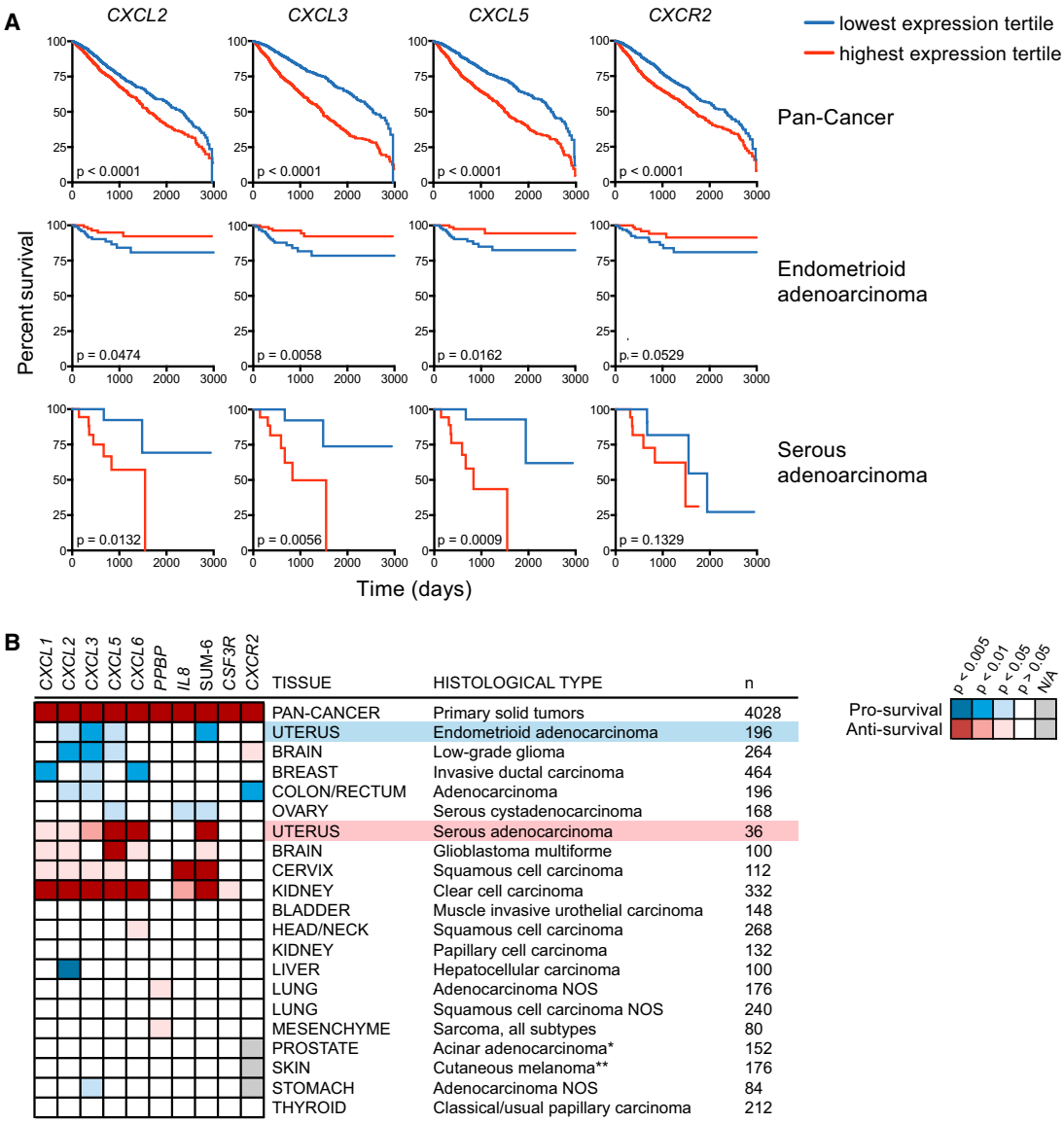

Figure 8. Relationship between a Tumor-Associated PMN Gene Signature and Survival Outcome in Human Cancers

(A) Patient survival with respect to the expression of four genes within the PMN signature. Survival was compared between patients whose primary tumors fell into the highest (red) versus lowest (blue) expression tertiles for the indicated gene. The Pan-Cancer analysis encompasses all patients with solid tumors.

(B) Heatmap extending the analysis from (A) to all PMN signature genes in many cancer subtypes. The blue and red colorings respectively indicate whether high expression of a gene was "pro-survival" or "anti-survival" based on the significance of the survival analysis. The white squares indicate no significant impact on survival ($p > 0.05$) and the gray squares indicate that analysis could not be performed due to negligible overall gene expression in that cancer subtype (n, number of samples within the high and low tertiles; *recurrence-free survival; **combined primary and metastatic cutaneous tumors).

See also Figure S8.

almost every other cancer subtype examined, individual ELR-CXC chemokine genes and SUM-6 demonstrated a strong positive expressional correlation with PMN-specific genes (Figures S8A–S8C), validating their use as reporters of PMN infiltration.

Combined analysis of all solid tumors (Pan-Cancer) revealed that elevated expression of each gene within the PMN signature correlated with reduced overall survival (Figure 8), consistent with the predominance of cancer literature connecting PMN accumulation with poor prognosis (Donskov, 2013). However, specific analysis of endometrioid EC showed that heightened expression of *CXCL2*, *CXCL3*, *CXCL5*, and SUM-6 significantly—and *CXCR2* ($p = 0.0529$) and *IL8* ($p = 0.0510$) nearly significantly—correlated with *improved* survival (Figure 8). Given the high 5-year survival rate (>80%) of endometrioid EC patients (Howlader et al., 2014), any statistically significant impact on survival can be considered remarkable. Survival benefits were likewise observed with another inflammatory gene (*CCL20*) and genes involved in PMN effector function—including ROS production (*CYBB* and *NCF1*) and tissue degradation (*MMP9*; Figure S8D)—all of which expectedly showed positive correlation

with the PMN signature (Figure S8E). These results suggested a pro-survival function for PMNs in human endometrioid EC, analogous to their pro-survival function in PRPL mice (Figure 5A). Moreover, the expression of ELR-CXC chemokine genes exhibited strong positive correlation with the expression of hypoxia-induced genes (Figure S8F), and functional annotation revealed that genes associated with the hypoxic response were significantly enriched ($p = 1.30 \times 10^{-5}$) in samples with high SUM-6 expression (data not shown). This link between inflammation and hypoxia was again consistent with our findings in the PRPL model and suggested that tumor-associated hypoxia might also promote PMN recruitment in human cancers.

Importantly, the correlation of an elevated PMN signature with improved survival was not unique to human endometrioid EC, but also applied to subtypes of brain, breast, colorectal, and ovarian cancer (Figure 8B). In contrast, a high PMN signature strongly correlated with reduced survival in several other cancers, including those of the brain, cervix, and kidney. This group also surprisingly included endometrial serous adenocarcinoma (serous EC; Figure 8), a pathologically distinct uterine cancer that is nevertheless derived from the same epithelial cells as endometrioid EC (Di Cristofano and Ellenson, 2007). The significance of this particular finding is discussed below. Lastly, the PMN signature had no obvious effect on survival in a number of additional cancer subtypes (Figure 8B), either suggesting that PMNs played no role in their progression or that PMN phenotype, rather than PMN numbers per se, influenced survival outcome.

DISCUSSION

Current work on PMNs in cancer consists of a growing chorus of publications that support a pro-tumorigenic role for these leukocytes, interspersed with select studies that hint at their converse potential to resist cancer development. Here, we unequivocally establish the ability of PMNs to oppose epithelial carcinogenesis. This demonstration involved two related autochthonous mouse models of uterine cancer and was supported by an analysis of TCGA data that revealed several human cancer subtypes including endometrioid EC in which PMNs might similarly impede cancer development. Importantly, our study did not employ transplantable tumors and, in contrast to other mouse models of cancer, describes PMNs acting as direct anti-tumor effectors in the absence of therapeutic manipulation and without contributions from cytotoxic T cells.

Our findings with respect to the mechanisms of tumor-associated PMN recruitment also stand in contrast to other mouse models of cancer. PMN recruitment in colorectal cancer models is thought to be driven by commensal microbes and tissue-resident myeloid and lymphoid cells (see Grivennikov et al., 2012) and in liver and prostate cancer models has been linked to the tumor cell-intrinsic senescence program (Kang et al., 2011; Toso et al., 2014). In the PRPL model, we systematically eliminated these possibilities and instead provided evidence that hypoxia was the cause of tumor cell inflammation and ensuing PMN infiltration. This evidence included the tight temporal and spatial correlation in vivo between tumor cell hypoxia, CXCL5 induction, and PMN accumulation, the hypoxic and highly inflamed phenotype of PRPL-*Csf3r*$^{-/-}$ tumors lacking PMNs, and the ability of hypoxia to induce ELR-CXC chemokine expression in isolated EC cells. A similar pathway for recruiting PMNs may be operative in human endometrioid EC, as tumors with a high PMN signature also showed elevated expression of several hypoxia-induced genes. The exact intracellular pathways that mediate ELR-CXC chemokine induction in EC cells remain to be defined, but they most likely involve both HIF-1α and NF-$\kappa\beta$ activation (Eltzschig et al., 2014). Importantly, PMNs can themselves promote tissue hypoxia via ROS production (Campbell et al., 2014) and can bolster their own recruitment via direct secretion of pro-inflammatory cytokines and chemokines (reviewed in Mantovani et al., 2011). Thus, while our results in the PRPL model clearly place hypoxia upstream of PMN recruitment, it remains possible that PMNs might further promote tissue hypoxia and inflammation after these processes are initially triggered.

Once recruited, we found that PMNs induce the basement membrane detachment of largely viable PRPL tumor cells (i.e., tumor cell sloughing) that then likely die within the uterine lumen. ELR-CXC chemokine production by hypoxic PRPL tumor cells thus appears to be part of a "debride me" signal that presumably has the physiological intent of restoring tissue homeostasis, but effectively reduces the pool of tumor cells capable of driving tumor growth and progression. Provocatively, our observations with the PL-AdCre model raise the possibility that PMN-induced tumor cell sloughing may, in certain circumstances, eradicate all of the cells of a nascent tumor and thus achieve tumor clearance. However, with larger tumors, sloughing likely generates a continuous wound-healing response in which new tumor cells replace the sloughed ones, an iterative stalemate that in turn may explain why PRPL tumor cells proliferate more rapidly in the presence of PMNs.

Interestingly, our data suggest that the debride me signal is also comprised in part of a ligand that activates PMNs in a MyD88-dependent manner. Given that antibiotics had no effect on the PRPL phenotype, this ligand is most likely one or more of the endogenous danger signals generated by stressed tumor cells that engage TLRs or the IL-1 receptor on PMNs, with PMN-derived IL-1β potentially acting in an autocrine amplifying loop. This activation step might also involve IL-18, though *Il18* expression was comparable in 4-week PL and PRPL uteri (data not shown). Importantly, MyD88-dependent activation was required for PMNs to disrupt the formation of stable α6β4-containing adhesion complexes in the BMZ, a feature of PRPL uteri that we in turn linked to the induction of tumor cell sloughing. Intriguingly, in mice and humans with genetic deficiencies in α6, β4, or other BMZ components, epithelial BMZ adhesion complex formation is globally disrupted, yet an additional, focal stimulus such as mechanical trauma is necessary to induce epithelial detachment (Zhang and Labouesse, 2010). This observation is consistent with the phenotype of PRPL uteri and suggests a two-step mechanism of PMN-induced tumor cell sloughing: initial BMZ adhesion complex disruption throughout the epithelium induced by diffusely infiltrating PMNs, followed by focal epithelial detachment in areas of high PMN density. We speculate that MyD88-dependent PMN activation might be involved in both of these steps through the induction of ROS and any number of the PMN-derived proteases known to degrade components of the epithelial BMZ, including neutrophil elastase and MMP-9 (Owen and Campbell, 1999; Riedle and Kerjaschki,

1997). Future work may help define the exact set of these factors relevant to the PRPL model and whether they act in unique or redundant fashion.

Intratumoral PMNs are commonly observed throughout all stages of progression in many human cancers, including endometrioid EC (Wallace et al., 2010). The surprising finding that PMNs can oppose tumorigenesis in endometrioid EC thus raises questions about what tumor-specific parameters influence their pro- versus anti-tumorigenic capacity. Most straightforwardly, tissue of origin might affect the ability of the tumor to recruit and activate PMNs or the susceptibility of the tumor to attack by PMNs and could certainly explain the discrepancy between our results from the PRPL model and those from other autochthonous tumor models that demonstrate clear pro-tumor roles for PMNs (Bald et al., 2014; Bongers et al., 2014; Houghton et al., 2010) and ELR-CXC chemokines (Jamieson et al., 2012; Katoh et al., 2013). Tumors derived from distinct cell subtypes within the same tissue might also respond differently to PMNs. For example, stromal tumors might be intrinsically resistant to PMN attack via the mechanisms described here because stromal cells do not rely upon basement membranes for survival. Moreover, cancer subtypes with the same tissue and cell of origin may be differentially impacted by PMNs based on tumor cell-intrinsic characteristics such as genetic makeup. This possibility is underscored by our findings with human serous EC, a less common subtype of uterine cancer derived from the same uterine epithelial cells as endometrioid EC, but with a vastly different genetic profile. Within the TCGA cohort, mutations in *PTEN* were far more common in endometrioid than in serous EC samples (79% versus 2%), while the reverse was true for *TP53* (13% versus 91%), consistent with the known biology of these two cancers. This observation implicates tumor genetics as a key determinant of the pro- versus anti-tumor character of PMNs; however, the anti-survival PMN signature of glioblastoma multiforme (31% *PTEN* mutations) and the pro-survival signature of ovarian cancer (95% *TP53* mutations) argue against the universality of this idea. Indeed, within endometrioid EC, a clear association between PTEN loss/AKT activation and recruitment of anti-tumor PMNs could not be established. Not only was AKT activation insufficient to induce ELR-CXC chemokine expression and PMN recruitment in the PRPL model (Figures 1L, S1A, and 6A), but analysis of an additional panel of PTEN-sufficient (HEC1A, HEC1B, and KLE) and PTEN-deficient (RL95-2) human EC lines revealed no obvious correlation between *PTEN* mutational status and either basal or hypoxia-induced *IL8* transcript levels (data not shown). In addition, pAKT protein levels in the endometrioid EC TCGA data set showed positive correlation with only a limited subset of our PMN and hypoxia signature genes (*CXCL2*, *CSF3R*, *CXCR2*, and *CA9*) and did not correlate with survival outcome (data not shown).

The discrepancy between endometrioid and serous EC might also result from the higher grade and more aggressive phenotype of serous EC (Di Cristofano and Ellenson, 2007). Tumor-associated PMNs might be inherently anti-tumorigenic in both cancer subtypes, but simply unable to combat tumorigenesis in serous EC due to its faster growth rate. PMN levels in serous EC might thus merely reflect the aggressiveness of each tumor rather than having a causal role in survival outcome. Interestingly, this tumor grade-based dichotomy finds a direct parallel in the impact of PMNs on low-grade versus high-grade gliomas (Figure 8B). The sheer capacity of a cancer to amass PMNs might also explain the difference between the two uterine cancer subtypes, in line with the idea that tumors with acute versus chronic inflammatory profiles may foster anti- versus pro-tumor PMNs, respectively (Souto et al., 2011). Indeed, serous EC showed lower overall expression of the PMN signature when compared to endometrioid EC (data not shown). Lastly, it is also possible that serous EC cells interact with their basement membrane in a way that renders them resistant to PMN attack.

Importantly, PMNs might simultaneously exert anti-tumorigenic and pro-tumorigenic effects within the same tumor, with net outcome dependent upon the tumor type and tumor stage. This duality was apparent within the PRPL model itself in that PMNs simultaneously promoted tumor cell sloughing and tumor cell proliferation. Additionally, the anti-tumor effects of PMNs may predominate mainly during the early stages of carcinogenesis, when tumor cells are expected to be more reliant on basement membrane attachment. Once this reliance is circumvented or the tumor simply grows too large to be resisted, the pro-tumor effects of PMNs documented in other systems may prevail (Brandau et al., 2013). Indeed, two recent lung cancer studies suggested that PMNs within early-stage tumors exerted stronger anti-tumor function than those within later stage tumors (Eruslanov et al., 2014; Mishalian et al., 2013). Clearly, the net effect of uterine PMN infiltration during the first 12 weeks of life in PRPL mice is to restrict tumor growth and progression, but this balance may be skewed differently in other cancers.

It remains to be seen whether tumor-associated PMNs can be manipulated therapeutically for patient benefit. CXCR2 antagonists that aim to minimize the pro-tumorigenic effects of PMNs by reducing their intratumoral numbers have shown promise in pre-clinical trials (reviewed in Dwyer and Yu, 2014). However, these agents may have limiting side effects such as diminished host defense against infection. Furthermore, the general feasibility of depleting tumor-associated PMNs is complicated by the fact that patients on chemotherapy routinely receive recombinant G-CSF to maintain blood neutrophil numbers. Therefore, stimulating the inherent anti-tumorigenic activities of PMNs might offer a more viable alternative. Indeed, a few recent clinical trials have pointed to the therapeutic utility of G-CSF administration (Souto et al., 2011). Our study provides a conceptual basis for such approaches by lending insight into the anti-tumor nature of PMNs.

EXPERIMENTAL PROCEDURES

Animals

PRPL ($Pgr^{cre/+}$ $Pten^{lox/lox}$) mice on a C57BL/6 background were generated in two separate ways. First, PRPL mice on a mixed background (Daikoku et al., 2008) were intercrossed with PL ($Pten^{lox/lox}$) mice on a C57BL/6 background (The Jackson Laboratory, Bar Harbor, ME, stock# 006440) for two generations, followed by the application of speed congenics (DartMouse) to select breeders with the highest amounts of C57BL/6 genomic DNA. These mice were then further backcrossed with C57BL/6 PL mice for more than four generations and then intercrossed to generate PRPL and PL controls. These PRPL and PL mice were used for experiments shown in Figures 1K, S2D–S2F, and 5A. After loss of this colony due to Hurricane Sandy, we regenerated the mice in collaboration with the Jackson Laboratory by intercrossing $Pgr^{cre/+}$ mice already on a C57BL/6 background (N = 5; the generous gift of Francesco DeMayo, Baylor College of Medicine, Houston, TX) with C57BL/6 PL mice.

These mice were used for all other experiments, including the intercrossing with C57BL/6-background strains of *Csf3r*$^{-/-}$, *Cxcr2*$^{-/-}$, *Myd88*$^{-/-}$, and *Trp53*$^{lox/lox}$ mice (Jackson, stock# 017838, 006848, 009088, and 008462, respectively), C57BL/6-background strains of *Flt3l*$^{-/-}$ and *Rag2*$^{-/-}$ mice (Taconic Biosciences, models 4207 and RAGN12, respectively), and a mixed C57BL6/C57BL10-background strain of *Rag2*$^{-/-}$*Il2rg*$^{-/-}$ mice (Taconic, model 4111). All colonies were maintained either at Jackson Laboratory or in specific pathogen-free animal barrier facilities at NYU School of Medicine and Memorial Sloan-Kettering Cancer Center (New York, NY). All animal experiments were approved by the Institutional Animal Care and Use Committee (IACUC) of the NYU Langone Medical Center and were conducted in accordance with the relevant regulatory standards.

TCGA Analysis

RNA-seq, whole exome sequencing, and protein expression databases were downloaded from the University of California-Santa Cruz Cancer Genomics Browser (https://genome-cancer.ucsc.edu/). For survival curve analysis, solid primary tumor sample RNA-seq data from patients with <3,000 days between initial diagnosis and event were sorted from lowest to highest expression of a given gene and divided into tertiles. The upper ("high expression") tertile was then directly compared to the lower ("low expression") tertile for survival analysis, while the middle tertile was excluded. For SUM-6, the sum of expression data from *CXCL1*, *CXCL2*, *CXCL3*, *CXCL5*, *CXCL6*, and *IL8* was calculated prior to sorting and division into tertiles. PMN-specific genes *CSF3R* and *FCGR3B* were selected based on exclusive expression of these genes within PMNs in the Garvan human immune cells database on the Immunological Genome Project Data Browser (http://www.immgen.org/databrowser/index.html) (Heng et al., 2008). These two genes, as well as *CXCR2*, have also been shown to be highly PMN-specific in humans using the recently described CIBERSORT algorithm (Newman et al., 2015). Some cancer subtypes that were included in Figure S7C, but not Figure 8B, had a sample size too small for a meaningful survival analysis. Genes in human endometrioid EC genes with significantly ($p < 0.05$) higher average expression in the SUM-6(high) versus the SUM-6(low) group were functionally annotated using the Database for Annotation, Visualization, and Integrated Discovery (DAVID; Broad Institute; https:/david.abcc.ncifcrf.gov/tools.jsp).

Statistical Analysis

All statistical analyses were performed in GraphPad Prism. For survival curve analysis, p values were calculated using the log rank test. For correlation of expression between two genes in TCGA human tumor samples, p values and the coefficient of determination (R^2) were determined by linear regression. For all other analyses, p values were determined using an unpaired two-tailed Student's t test. Statistical significance was defined as $p < 0.05$.

Additional Procedures

These are described in the online Supplemental Information.

ACCESSION NUMBERS

The accession number for the RNA-seq data reported in the paper is GEO: GSE73541.

SUPPLEMENTAL INFORMATION

Supplemental Information includes Supplemental Experimental Procedures and eight figures and can be found with this article online at http://dx.doi.org/10.1016/j.ccell.2015.11.005.

ACKNOWLEDGMENTS

We thank G. David, K. Cadwell, R. Possemato, E. Hernando, E. Maltepe, A. Frey, and J. Handler for discussions and assistance and F. DeMayo for mice. Histopathology, Genome Technology, and Cytometry and Cell Sorting Core facilities were supported in part by grant P30CA016087 from the National Cancer Institute. Supported by NIH grants RO1CA168755 to A.E., HD068524 and PO1CA7783 to S.K.D., and F30CA165385 to A.B. A.C. was supported in part by a prize from the The Bettencourt-Schueller Foundation.

Received: March 11, 2015
Revised: August 20, 2015
Accepted: November 17, 2015
Published: December 14, 2015

REFERENCES

Albanesi, M., Mancardi, D.A., Jönsson, F., Iannascoli, B., Fiette, L., Di Santo, J.P., Lowell, C.A., and Bruhns, P. (2013). Neutrophils mediate antibody-induced antitumor effects in mice. Blood *122*, 3160–3164.

Bald, T., Quast, T., Landsberg, J., Rogava, M., Glodde, N., Lopez-Ramos, D., Kohlmeyer, J., Riesenberg, S., van den Boorn-Konijnenberg, D., Hömig-Hölzel, C., et al. (2014). Ultraviolet-radiation-induced inflammation promotes angiotropism and metastasis in melanoma. Nature *507*, 109–113.

Beauparlant, S.L., Read, P.W., and Di Cristofano, A. (2004). In vivo adenovirus-mediated gene transduction into mouse endometrial glands: a novel tool to model endometrial cancer in the mouse. Gynecol. Oncol. *94*, 713–718.

Bongers, G., Pacer, M.E., Geraldino, T.H., Chen, L., He, Z., Hashimoto, D., Furtado, G.C., Ochando, J., Kelley, K.A., Clemente, J.C., et al. (2014). Interplay of host microbiota, genetic perturbations, and inflammation promotes local development of intestinal neoplasms in mice. J. Exp. Med. *211*, 457–472.

Brandau, S., Dumitru, C.A., and Lang, S. (2013). Protumor and antitumor functions of neutrophil granulocytes. Semin. Immunopathol. *35*, 163–176.

Campbell, E.L., Bruyninckx, W.J., Kelly, C.J., Glover, L.E., McNamee, E.N., Bowers, B.E., Bayless, A.J., Scully, M., Saeedi, B.J., Golden-Mason, L., et al. (2014). Transmigrating neutrophils shape the mucosal microenvironment through localized oxygen depletion to influence resolution of inflammation. Immunity *40*, 66–77.

Chen, Z., Trotman, L.C., Shaffer, D., Lin, H.K., Dotan, Z.A., Niki, M., Koutcher, J.A., Scher, H.I., Ludwig, T., Gerald, W., et al. (2005). Crucial role of p53-dependent cellular senescence in suppression of Pten-deficient tumorigenesis. Nature *436*, 725–730.

Colgan, S.P., Dzus, A.L., and Parkos, C.A. (1996). Epithelial exposure to hypoxia modulates neutrophil transepithelial migration. J. Exp. Med. *184*, 1003–1015.

Coppé, J.P., Desprez, P.Y., Krtolica, A., and Campisi, J. (2010). The senescence-associated secretory phenotype: the dark side of tumor suppression. Annu. Rev. Pathol. *5*, 99–118.

Daikoku, T., Hirota, Y., Tranguch, S., Joshi, A.R., DeMayo, F.J., Lydon, J.P., Ellenson, L.H., and Dey, S.K. (2008). Conditional loss of uterine Pten unfailingly and rapidly induces endometrial cancer in mice. Cancer Res. *68*, 5619–5627.

Daikoku, T., Terakawa, J., Hossain, M.M., Yoshie, M., Cappelletti, M., Yang, P., Ellenson, L.H., and Dey, S.K. (2014). Mammalian target of rapamycin complex 1 and cyclooxygenase 2 pathways cooperatively exacerbate endometrial cancer. Am. J. Pathol. *184*, 2390–2402.

Di Cristofano, A., and Ellenson, L.H. (2007). Endometrial carcinoma. Annu. Rev. Pathol. *2*, 57–85.

Donskov, F. (2013). Immunomonitoring and prognostic relevance of neutrophils in clinical trials. Semin. Cancer Biol. *23*, 200–207.

Dwyer, M.P., and Yu, Y. (2014). CXCR2 receptor antagonists: a medicinal chemistry perspective. Curr. Top. Med. Chem. *14*, 1590–1605.

Eltzschig, H.K., Bratton, D.L., and Colgan, S.P. (2014). Targeting hypoxia signalling for the treatment of ischaemic and inflammatory diseases. Nat. Rev. Drug Discov. *13*, 852–869.

Eruslanov, E.B., Bhojnagarwala, P.S., Quatromoni, J.G., Stephen, T.L., Ranganathan, A., Deshpande, C., Akimova, T., Vachani, A., Litzky, L., Hancock, W.W., et al. (2014). Tumor-associated neutrophils stimulate T cell responses in early-stage human lung cancer. J. Clin. Invest. *124*, 5466–5480.

Fridlender, Z.G., Sun, J., Kim, S., Kapoor, V., Cheng, G., Ling, L., Worthen, G.S., and Albelda, S.M. (2009). Polarization of tumor-associated neutrophil phenotype by TGF-beta: "N1" versus "N2" TAN. Cancer Cell *16*, 183–194.

Granot, Z., Henke, E., Comen, E.A., King, T.A., Norton, L., and Benezra, R. (2011). Tumor entrained neutrophils inhibit seeding in the premetastatic lung. Cancer Cell *20*, 300–314.

Grivennikov, S.I., Wang, K., Mucida, D., Stewart, C.A., Schnabl, B., Jauch, D., Taniguchi, K., Yu, G.Y., Osterreicher, C.H., Hung, K.E., et al. (2012). Adenoma-linked barrier defects and microbial products drive IL-23/IL-17-mediated tumour growth. Nature *491*, 254–258.

Heng, T.S., and Painter, M.W.; Immunological Genome Project Consortium (2008). The Immunological Genome Project: networks of gene expression in immune cells. Nat. Immunol. *9*, 1091–1094.

Houghton, A.M., Rzymkiewicz, D.M., Ji, H., Gregory, A.D., Egea, E.E., Metz, H.E., Stolz, D.B., Land, S.R., Marconcini, L.A., Kliment, C.R., et al. (2010). Neutrophil elastase-mediated degradation of IRS-1 accelerates lung tumor growth. Nat. Med. *16*, 219–223.

Howlader, N., Noone, A.M., Krapcho, M., Garshell, J., Miller, D., Altekruse, S.F., Kosary, C.L., Yu, M., Ruhl, J., Tatalovich, Z., et al. (2014). SEER cancer statistics review, 1975-2011, National Cancer Institute. Bethesda, MD, http://seer.cancer.gov/csr/1975_2011/, based on November 2013 SEER data submission, posted to the SEER web site, April 2014.

Jamieson, T., Clarke, M., Steele, C.W., Samuel, M.S., Neumann, J., Jung, A., Huels, D., Olson, M.F., Das, S., Nibbs, R.J., and Sansom, O.J. (2012). Inhibition of CXCR2 profoundly suppresses inflammation-driven and spontaneous tumorigenesis. J. Clin. Invest. *122*, 3127–3144.

Johnston, R.A., Mizgerd, J.P., and Shore, S.A. (2005). CXCR2 is essential for maximal neutrophil recruitment and methacholine responsiveness after ozone exposure. Am. J. Physiol. Lung Cell. Mol. Physiol. *288*, L61–L67.

Kang, T.W., Yevsa, T., Woller, N., Hoenicke, L., Wuestefeld, T., Dauch, D., Hohmeyer, A., Gereke, M., Rudalska, R., Potapova, A., et al. (2011). Senescence surveillance of pre-malignant hepatocytes limits liver cancer development. Nature *479*, 547–551.

Katoh, H., Wang, D., Daikoku, T., Sun, H., Dey, S.K., and Dubois, R.N. (2013). CXCR2-expressing myeloid-derived suppressor cells are essential to promote colitis-associated tumorigenesis. Cancer Cell *24*, 631–644.

Kousis, P.C., Henderson, B.W., Maier, P.G., and Gollnick, S.O. (2007). Photodynamic therapy enhancement of antitumor immunity is regulated by neutrophils. Cancer Res. *67*, 10501–10510.

Liu, F., Wu, H.Y., Wesselschmidt, R., Kornaga, T., and Link, D.C. (1996). Impaired production and increased apoptosis of neutrophils in granulocyte colony-stimulating factor receptor-deficient mice. Immunity *5*, 491–501.

Liu, Z., Shapiro, S.D., Zhou, X., Twining, S.S., Senior, R.M., Giudice, G.J., Fairley, J.A., and Diaz, L.A. (2000). A critical role for neutrophil elastase in experimental bullous pemphigoid. J. Clin. Invest. *105*, 113–123.

Mantovani, A., Cassatella, M.A., Costantini, C., and Jaillon, S. (2011). Neutrophils in the activation and regulation of innate and adaptive immunity. Nat. Rev. Immunol. *11*, 519–531.

Mishalian, I., Bayuh, R., Levy, L., Zolotarov, L., Michaeli, J., and Fridlender, Z.G. (2013). Tumor-associated neutrophils (TAN) develop pro-tumorigenic properties during tumor progression. Cancer Immunol. Immunother. *62*, 1745–1756.

Molloy, M.J., Grainger, J.R., Bouladoux, N., Hand, T.W., Koo, L.Y., Naik, S., Quinones, M., Dzutsev, A.K., Gao, J.L., Trinchieri, G., et al. (2013). Intraluminal containment of commensal outgrowth in the gut during infection-induced dysbiosis. Cell Host Microbe *14*, 318–328.

Newman, A.M., Liu, C.L., Green, M.R., Gentles, A.J., Feng, W., Xu, Y., Hoang, C.D., Diehn, M., and Alizadeh, A.A. (2015). Robust enumeration of cell subsets from tissue expression profiles. Nat. Methods *12*, 453–457.

Owen, C.A., and Campbell, E.J. (1999). The cell biology of leukocyte-mediated proteolysis. J. Leukoc. Biol. *65*, 137–150.

Prince, L.R., Whyte, M.K., Sabroe, I., and Parker, L.C. (2011). The role of TLRs in neutrophil activation. Curr. Opin. Pharmacol. *11*, 397–403.

Riedle, B., and Kerjaschki, D. (1997). Reactive oxygen species cause direct damage of Engelbreth-Holm-Swarm matrix. Am. J. Pathol. *151*, 215–231.

Souto, J.C., Vila, L., and Brú, A. (2011). Polymorphonuclear neutrophils and cancer: intense and sustained neutrophilia as a treatment against solid tumors. Med. Res. Rev. *31*, 311–363.

Tagliani, E., Shi, C., Nancy, P., Tay, C.S., Pamer, E.G., and Erlebacher, A. (2011). Coordinate regulation of tissue macrophage and dendritic cell population dynamics by CSF-1. J. Exp. Med. *208*, 1901–1916.

Toso, A., Revandkar, A., Di Mitri, D., Guccini, I., Proietti, M., Sarti, M., Pinton, S., Zhang, J., Kalathur, M., Civenni, G., et al. (2014). Enhancing chemotherapy efficacy in Pten-deficient prostate tumors by activating the senescence-associated antitumor immunity. Cell Rep. *9*, 75–89.

Trinchieri, G. (2012). Cancer and inflammation: an old intuition with rapidly evolving new concepts. Annu. Rev. Immunol. *30*, 677–706.

Venaille, T.J., Mendis, A.H., Phillips, M.J., Thompson, P.J., and Robinson, B.W. (1995). Role of neutrophils in mediating human epithelial cell detachment from native basement membrane. J. Allergy Clin. Immunol. *95*, 597–606.

Wallace, A.E., Gibson, D.A., Saunders, P.T., and Jabbour, H.N. (2010). Inflammatory events in endometrial adenocarcinoma. J. Endocrinol. *206*, 141–157.

Weigelt, B., Warne, P.H., Lambros, M.B., Reis-Filho, J.S., and Downward, J. (2013). PI3K pathway dependencies in endometrioid endometrial cancer cell lines. Clin. Cancer Res. *19*, 3533–3544.

Zhang, H., and Labouesse, M. (2010). The making of hemidesmosome structures in vivo. Dev. Dyn. *239*, 1465–1476.